stellarator news

Published by Fusion Energy Division, Oak Ridge National Laboratory
Building 9201-2; P.O. Box 2009; Oak Ridge, TN 37831-8071, USA
Editor: James A. Rome
Issue #23 September, 1992
E-Mail:Rome@fed.ornl.gov

Around the Labs

H-mode-like transitions in W7-AS

The last high-field campaign at 2.5 T with 140-GHz ECRH on W7-AS gave rise to additional doses of adrenalin in the veins, particularly of those who have watched H-mode developments in ASDEX over nearly 10 years. W7-AS produced traces of astonishing similarity to those on ASDEX in the H-mode. In this report, I will try to compare our findings on W7-AS with the known H-mode characteristics from tokamaks.

Figure 1 compares β_{pol}, line-averaged density, and H_α within the divertor chamber during a beam heating phase of ASDEX with the energy content, line density, and H_α measured at the top limiter of W7-AS during 140-GHz ECRH. In both cases, there is a transition which is clearly shown by the H_α traces. For ASDEX, the temporal development of H_α shows the known symmetry in transition regimes, OH → L → H → L → OH; the W7-AS H_α trace also indicates a transition and a back-transition when the ECRH pulse is turned off. The feature of the back-transition is not as pronounced as on ASDEX because the plasma decays as soon as the heating is turned off and is not maintained by Ohmic heating (the last short peak in the H_α trace from W7-AS originates from recombination and is not related to the confinement). In both ASDEX and W7-AS, the H_α signal is modulated by additional activity identified as edge localized modes (ELMs) in tokamaks.

The changes in confinement are characterized by the rise in energy and particle content. The back-transition is accompanied by a phase of enhanced transport: in some cases a steepening of the slope of the decaying electron temperature could be noted at that moment. The amount by which energy and particle confinement improve is clearly lower than on ASDEX and is discussed below.

Figure 2 is a collection of H_α traces from W7-AS and indicates the somewhat erratic nature with which the H-

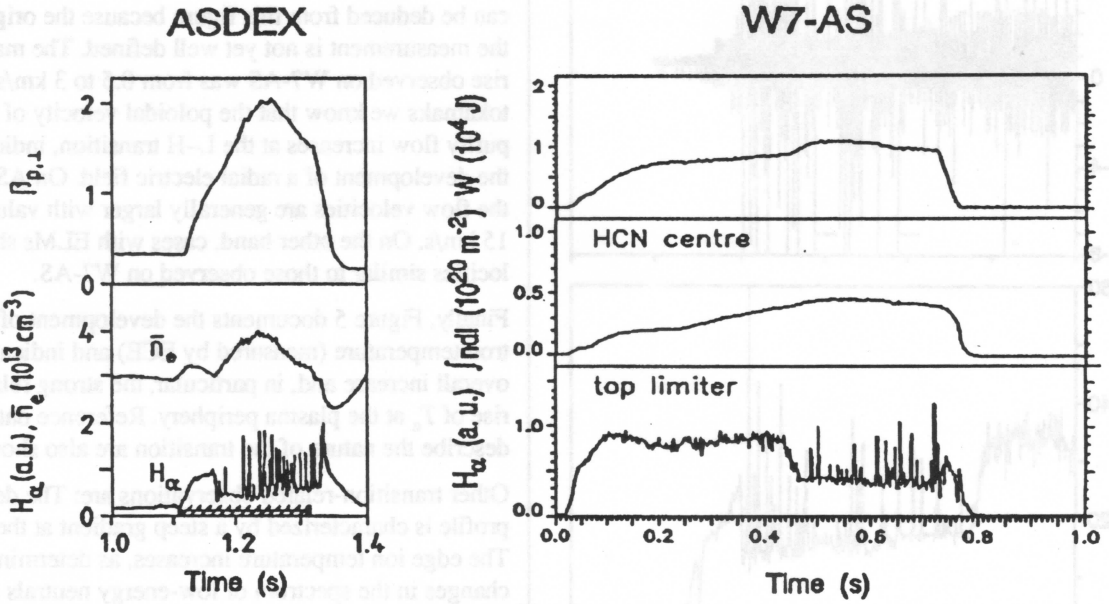

Fig. 1.

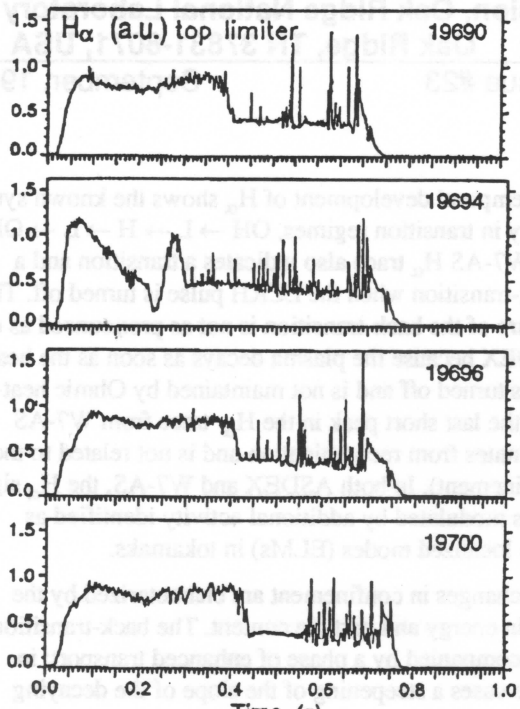

Fig. 2.

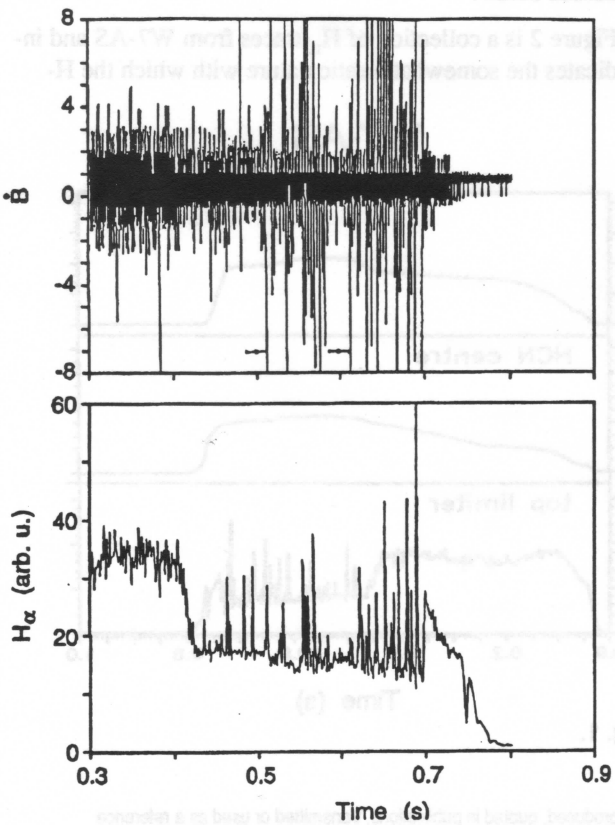

Fig. 3.

mode-like transitions occur. Again, this is similar to the experience on tokamaks. The specific purpose of this study was to assess the role of the external gas flow on the transition and on the confinement quality prior to it.

Figure 3 shows a trace from one Mirnov loop on W7-AS along with the H_α trace for orientation. Correlated with the reduction and the following increase in H_α is a reduction and followed by an increase in the magnetic turbulence. Such a change is also known from tokamaks; in particular, DIII-D showed evidence of a correlated change in the magnetic turbulence level in the H-mode.

The bursts appearing in H_α on W7-AS after the transition are attributed to instabilities localized at the plasma periphery. Like the ELMs in ASDEX, they give rise to a loss of particles and energy. The pivot point, as deduced from soft X ray radiation, is about 3 cm inside the last closed flux surface (ASDEX: 4 cm). In accordance with the ELM activity on ASDEX, the beta loss is caused by a short, highly turbulent phase of 200–300 μs duration (ASDEX: 400 μs). ELMs in ASDEX have a short MHD precursor in the frequency range of 100–200 kHz. In only a few cases, short precursors at high frequency close to the limits of resolution have been observed on W7-AS.

Figure 4 shows preliminary measurements of the poloidal velocity of B IV at the plasma edge. At the transition, the poloidal velocity increases in the direction of the electron diamagnetic drift. Only relative information can be deduced from this figure because the origin for the measurement is not yet well defined. The maximum rise observed on W7-AS was from 0.5 to 3 km/s. On tokamaks we know that the poloidal velocity of the impurity flow increases at the L–H transition, indicating the development of a radial electric field. On ASDEX the flow velocities are generally larger with values up to 15 km/s. On the other hand, cases with ELMs show velocities similar to those observed on W7-AS.

Finally, Figure 5 documents the development of the electron temperature (measured by ECE) and indicates the overall increase and, in particular, the strong relative rise of T_e at the plasma periphery. Reference data which describe the nature of the transition are also shown.

Other transition-related observations are: The density profile is characterized by a steep gradient at the edge. The edge ion temperature increases, as determined from changes in the spectrum of low-energy neutrals as measured by time of flight. Similar changes in the flux spectra are observed on ASDEX with the same diagnostic. These observations clearly indicate the development of an edge transport barrier. Furthermore, the impurity con-

centration increases after the transition. The line radiation of impurities injected prior to the transition stops decaying as soon as the transition occurs. All these parameter changes are in qualitative agreement with similar observations in tokamaks at the L–H transition.

The H-mode-like transitions were observed for the first time on W7-AS during high-density operation with ECRH at 140 GHz under boronized wall conditions and at $\iota \approx 0.52$. The impact of the limiter on the plasma edge properties is reduced at this iota value, and the last closed flux surface is at least partly determined by the separatrix. As with the H-mode in tokamaks, the proximity of the limiter has a deleterious effect. It has been demonstrated that the H-mode-like transition can be suppressed in W7-AS when the plasma aperture is reduced by the movable limiter and the LCFS is determined by it.

There is a density limit — however not too well established — of about 5×10^{13} cm^{-3} which is higher than that in tokamaks ($\approx 2 \times 10^{13}$ cm^{-3}). The density limit is close to the cut-off density of the 70-GHz system of W7-AS. There is also a power threshold. This is already indicated by the existence of a back-transition. The necessary power flux across the LCFS agrees roughly with that on tokamaks at the L-H transition.

The observation of H-mode-like transitions in W7-AS initiated a survey of older W7-AS discharges. This is important, as the development of stellarator plasmas of the shearless type represented by the Wendelstein line allows spontaneous transitions which affect both energy and particle confinement. These transitions are caused by configurational changes induced by changes in the profile of the equilibrium currents. Traces with H_α-bursts but without clear transitions were indeed observed with NBI and ECRH at 70 GHz (close to cut-off). These observations confirm the limitation of the operational range to higher iota values. They also confirm the development of steep edge density profiles.

The H-mode-like transitions of W7-AS deviate from the H-mode observed in divertor tokamaks in the extent to which confinement improves. The highest increases in the energy content in W7-AS of about 30% were achieved with an added vertical field, giving rise to an inward shift of the plasma column. The confinement times in the H-mode-like phases are about 30 ms. The difference from the tokamak divertor case might be the deleterious impact of the W7-AS limiter. It is known from ASDEX, and better documented on TFTR, that limiter-dominated H-modes have only a marginal improvement in τ_E. Also, according to TFTR, the L–H transition does not occur as rapidly as in the case of a clean divertor H-mode transition. One can only speculate about the reason: Enhanced charge-exchange losses

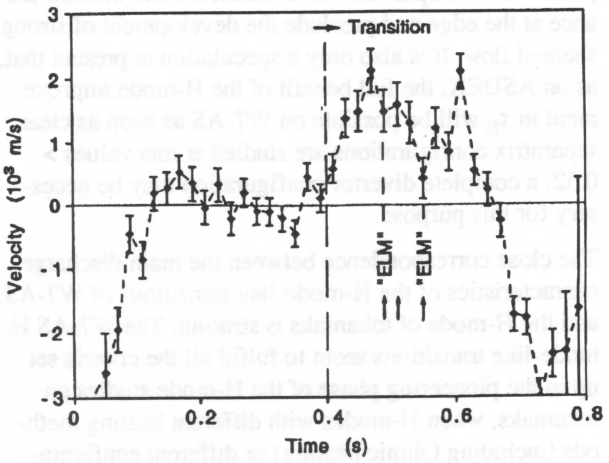

Fig. 4

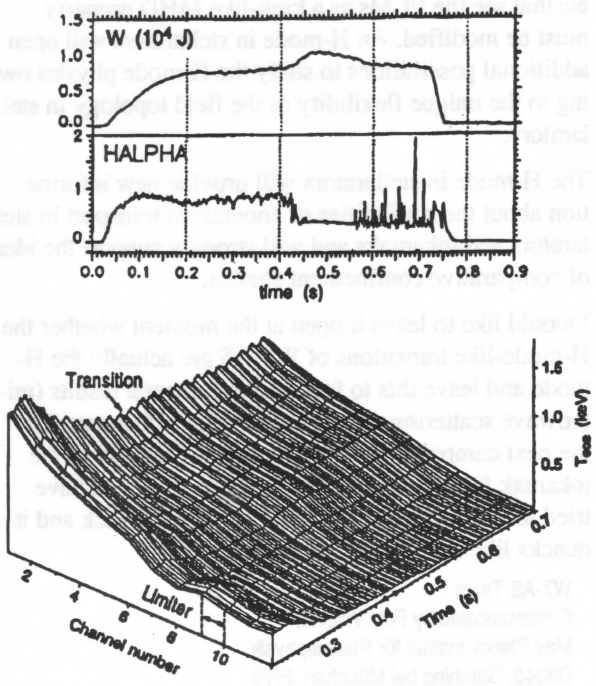

Fig. 5.

at the plasma edge could either reduce the beneficial impact of the transport barrier or affect the momentum balance at the edge and preclude the development of strong sheared flow. It is also only a speculation at present that, as on ASDEX, the full benefit of the H-mode improvement in τ_E will be possible on W7-AS as soon as clear separatrix configurations are studied at iota values > 0.52; a complete divertor configuration may be necessary for this purpose.

The close correspondence between the main discharge characteristics of the H-mode-like transitions of W7-AS and the H-mode of tokamaks is striking. The W7-AS H-mode-like transitions seem to fulfill all the criteria set up in the pioneering phase of the H-mode studies on tokamaks, when H-modes with different heating methods (including Ohmic heating) or different configurations (limiter versus divertor) or different plasma scenarios (current ramps) had to be sorted out and categorized.

The claim that H-modes are also possible in stellarators has, however, a different quality than the realization of the H-mode in a tokamak in a novel operational scenario. The impact on the H-mode physics will be strong — for both the H-mode transition and the ELM physics. Models that link the H-mode to specific shapes of the toroidal current profile (owing to the high electrical conductivity at the edge) must be reconsidered. Also, models that see the ELMs as a kink-like MHD property must be modified. An H-mode in stellarators will open additional possibilities to study the H-mode physics owing to the unique flexibility of the field topology in stellarators.

The H-mode in stellarators will provide new information about the similarities of anomalous transport in stellarators and tokamaks and will strongly support the idea of comparative confinement studies.

I would like to leave it open at the moment whether the H-mode-like transitions of W7-AS are actually the H-mode and leave this to further experimental results (microwave scattering at the plasma edge is foreseen for the next campaign) and future discussions within the tokamak family of H-mode operators. But, as I have tried to convince the reader, it walks like a duck and it quacks like a duck and therefore...

W7-AS Team
Communicated by Fritz Wagner
Max Planck Institut für Plasmaphysik
D8046, Garching bei München, FRG
Phone (49)-89-3299-1963
FAX (49)-89-3299-2584

Electron density and floating potential fluctuations in Wendelstein 7-AS and ASDEX

A comparison of electron density and floating potential fluctuations measured with a reciprocating Langmuir probe array of 19 graphite tips in the edge plasma of the Wendelstein 7-AS stellarator and the ASDEX tokamak has shown that the fluctuation levels, the phase propagation velocity of the fluctuations, and the spatial correlation of the density and potential fluctuations have many features in common [1,2].

A radial scan of the reciprocating Langmuir probe through 10 cm in 150 ms provides the radial profiles of the mean and rms values of the measured quantities. Discharges with 200 of kW ECRH power and $n_e = 2 \times 10^{19}$ m^{-3} at $B_0 = 1.28$ T in W7-AS and Ohmic discharges with $n_e = 2.9 \times 10^{19}$ m^{-3} at $B_0 = 1.28$ T in ASDEX were studied. In these discharges, the electron temperature at the last closed flux surface (approximately 20 eV) and the fall-off length (2.1 cm) were similar, but the electron densities in W7-AS were lower (0.25×10^{19} m^{-3} vs 0.40×10^{19} m^{-3}) and the fall-off lengths were steeper (1.7 cm vs 2.2 cm).

The normalized fluctuation level of the saturation current I_{sat} decreases with decreasing minor radius in both machines with a typical value of 0.20–0.25 at $r/a = 1$. In both machines, the sharp dip in the floating potential at the limiter (W7-AS) or separatrix (ASDEX) position and the decrease in plasma temperature with minor radius lead to a plasma potential profile with a maximum in the vicinity of $r/a = 1$. In the experiments on W7-AS, one of the two limiters was stepped inwards to clearly demonstrate that the limiter position determines the location of the observed dip in floating potential. The peaking of the plasma potential in the vicinity of $r/a = 1$ leads to a reversal of the radial electric field at this position. The observed inversion of the direction of poloidal propagation agrees well with estimates of the $\boldsymbol{E} \times \boldsymbol{B}$-induced drift of the fluctuations. The presence of such a velocity shear layer in both machines shows that such a feature is independent of plasma current and magnetic field shear, since W7-AS is a current-free low-shear stellarator.

Shown in Fig. 1 is a contour plot of the cross-correlation found between the floating potential and the ion saturation current as a function of the poloidal separation between the probe tips in both machines. The cross-correlation of two signals, for a time shift, τ, of one of the signals, has a value of 1 when the signals are perfectly correlated with a zero phase shift and a value

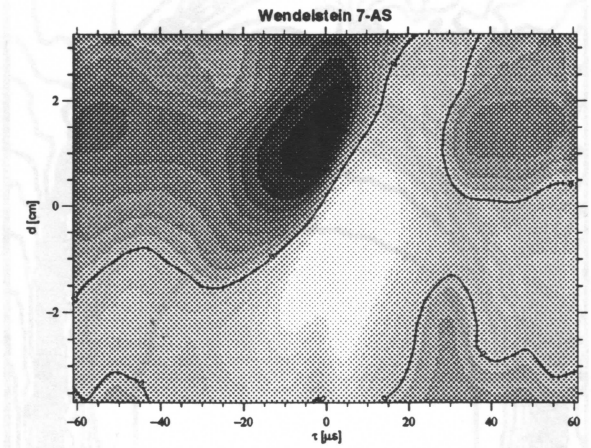

(a)

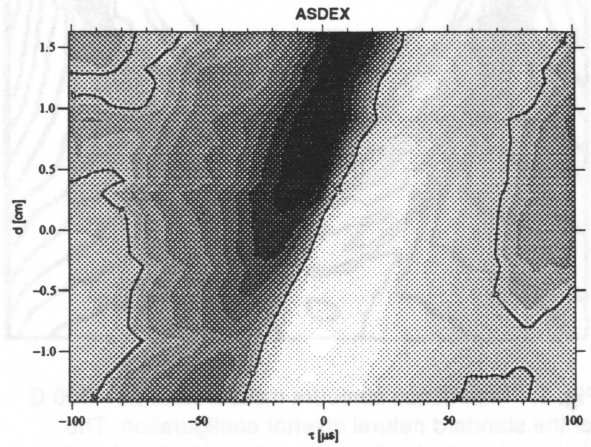

(b)

Fig. 1. Contour plot of the degree of cross-correlation between fluctuations in floating potential and ion saturation current as a function of the poloidal separation between the tips (a) on W&-AS and (b) on ASDEX. The horizontal axis is the time shift, τ, between the signals. The phase velocity of the fluctuations in the poloidal direction is the reason for the skewed nature of the contour plots.

of -1 when the signals are perfectly correlated but are phase shifted by 180°. Uncorrelated signals have a value of zero. In the contour plot, the lighter regions correspond to the 'in-phase' cross-correlation, and the dark regions correspond to the 'out-of-phase' cross-correlation. A cross-correlation maximum is found when the poloidal separation between the tips measuring the floating potential and ion saturation current fluctuation is about 1 cm in both the stellarator and the tokamak.

A turbulent eddy model has been proposed to explain this observation. In the presence of a density gradient, a local potential hill induces an $\boldsymbol{E} \times \boldsymbol{B}$ drift that pushes plasma of higher (lower) density onto tips in front of (behind) the potential maximum. The cross-correlation maximum (minimum) is then found on the dominant spatial scale of the turbulent eddies. Modeling of the edge turbulence as a random superposition of eddies is being carried out. With appropriate choices of the shape and size distribution of the structures, a satisfactory agreement between the simulations and experiment is found.

The development of a two-dimensional model of the scrape-off layer, including the boundary conditions imposed by the presence of a target plate or limiter, is in progress. This numerical treatment will be compared with the experimental results.

[1] R. Balbin, A. Carlson, M. Endler, L. Giannone, G. Herre, C. Hidalgo, H. Niedermeyer, A. Rudyj, G. Theimer, W7-AS Team and ASDEX Team, 19th EPS Conference on Controlled Fusion and Plasma Physics (Innsbruck), Vol. II, p. 783,1992.

[2] M. Endler, G. Theimer, M. Weinlich, A. Carlson, L. Giannone, H. Niedermeyer, A. Rudyj and ASDEX Team, 19th EPS Conference on Controlled Fusion and Plasma Physics (Innsbruck), Vol. II, p. 787, 1992.

Louis Giannone for the Fluctuation Group (W7-AS)
Max Planck Institut für Plasmaphysik
D8046, Garching bei Muenchen, FRG
Phone (49)-89-3299-1499
FAX (49)-89-3299-2584

Magnetic surface mapping of Heliotron-E

The Heliotron-E vacuum magnetic field has a rotational transform ($0.52 < \iota < 2.5$) that is sensitive to a low-mode perturbation field, and therefore one of the targets for Heliotron-E plasma confinement improvement was to explore ways to control these potentially dangerous resonances in addition to the built-in strong magnetic shear that is the main countermeasure [1]. A small toroidal field can add a shallow magnetic well, which leads to a possible stabilization of inherent microinstabilities. An inward magnetic axis shift can contribute to the restoration of helical symmetry for orbit control, as well as to increase the magnetic shear.

In connection with these configuration control studies, the full two-dimensional (2-D) scan of the flux-surface mapping is particularly beneficial to develop a better understanding of the plasma confinement characteristics in Heliotron-E because of the direct observation of the vacuum separatrix as well as the incidental island topology. Concerning the desirability of the magnetic surface control, the key elements of our study were the effects of (i) the magnetic axis shift, (ii) the applied toroidal field (the a^* effects), (iii) the superimposed perturbation field (e.g., by means of the $m = 1$, $n = 1$ island formation coils), and (iv) the insertion of a rail-type carbon limiter inside the separatrix.

The surface mapping that was performed was based on the well-known "stellarator diode" method, but we adopted the "directed electron beam" method rather than the conventional "emissive filament" method. One feature of this method was the comparatively high reliability of determining the vacuum magnetic surface impedance independently of the electron-gun emission properties. The tiny electron gun could be scanned in steps of less than 1 mm, horizontally and/or vertically, at a fixed toroidal angle (port number 5.5). The observed range of the vacuum impedance was on the order of 1–30 MΩ inside the determined separatrix under the DC 500-G main magnetic field at 2×10^{-8} Torr conditions, and therefore we could observe the $\iota = 1$ island that was vulnerable to the earth's magnetic field. These 2-D mapping results can furnish definite and reliable information about the high-field vacuum magnetic structure with predictable extrapolation as well as information about the origins of the probable external error fields. Previous 1-D scan measurements suggested the presence of a low-level magnetic braiding ($\iota > 2$), an $\iota = 1$ island, etc [2–4].

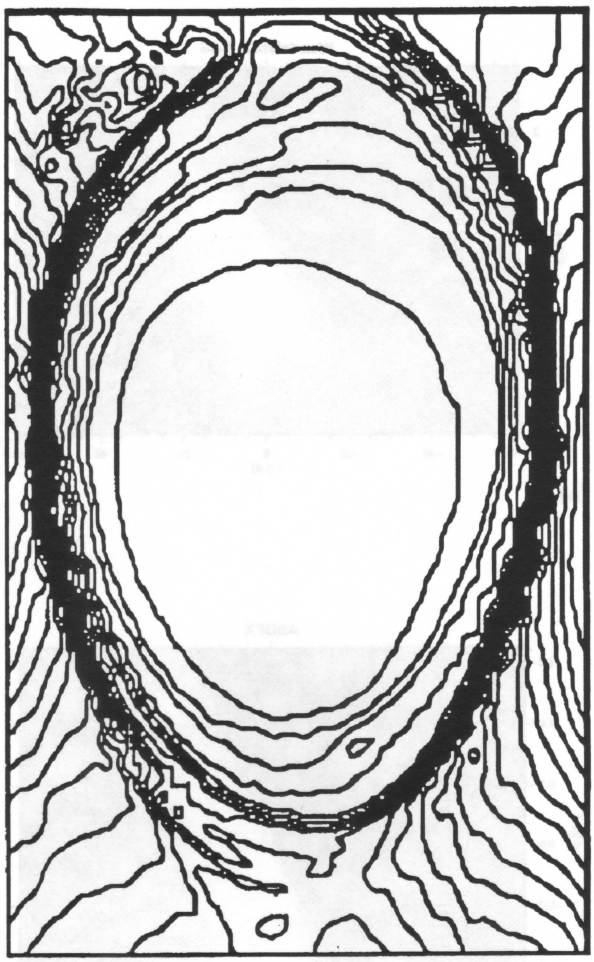

Fig. 1. Impedance contours measured at $B_h = 500$ G for the standard natural divertor configuration. The observed $\iota = 1$ island can be reduced in the high-field plasma experiments.

The objective of the present study is to deal with a more detailed 2-D topological analysis of the magnetic field structure. The location of the separatrix provides a sensitive measure of the diagnostic accuracy when compared with numerical field-line tracing. The observed impedance contour characteristics revealed the evident structure of the closed, nested magnetic flux surfaces (more correctly, drift surfaces of the directed 15-eV electrons) inside the separatrix. Although the determined separatrix radius is slightly less than the original design value for the standard configuration, no apparent anomalies except for the $\iota = 1$ island due mainly to the earth's magnetic field were seen in the core region within the present detection level, as shown in Fig. 1.

On the other hand, detailed analysis of the ergodicity of the separatrix layer and of the presence of "natural" and/or "induced" magnetic islands at the edge, as well as of their removal by the error-correcting fields, will be of special importance. In this connection, the poisonous effect of the $m = 1$, $n = 1$ superimposed perturbation field (e.g., $B_{1,1}/B_0 = 6 \times 10^{-4}$) was studied in order to check the response of the magnetic lines of force, and the measured result was in general accordance with the prediction in terms of both the island phase topology and the island width [5]. It was also confirmed that the a^* application can expand or shrink the separatrix radius depending on its sign and that the determined magnetic axis can be shifted in accordance with the calculation. Moreover, limiter insertion was found to modify the nested surface structure in terms of the corresponding connection length.

The detailed analysis of the probable error fields other than the earth's magnetic field still remains in the present preliminary phase, but this method was found to have marked potential for solving that problem, and now we are preparing for the next, more detailed experiments.

F. Sano for the Heliotron-E Group
Plasma Physics Laboratory
Kyoto University
Gokasho,Uji 611, Japan
FAX 81774330865

[1] F. Sano et al., Nucl. Fusion **30** (1990) 81; F. Sano et al., 1st Int. Toki Conference on Plasma Physics and Controlled Nuclear Fusion Research 1989, NIFS-PROC-3, 192.
[2] T. Obiki et al., Plasma Physics and Controlled Nuclear Fusion Research 1990, Vol. 2 (IAEA,Vienna, 1991) 425.
[3] R. Takahashi et al., Jpn. J. Appl. Phys. **28** (1989) 2604.
[4] T. Mizuuchi et al., J. Nucl. Mater. **176 &177** (1990)1070.
[5] F. Sano et al., 1992 Int. Conf. Plasma Physics, Innsbruck, July 1992, Vol. I, 489.

Effects of magnetic field perturbations in the ATF torsatron

The effects of errors in the magnetic fields of tokamaks on the plasma are quite different from those in stellarators. In tokamaks, field errors can cause disruptive locked modes [1–3] through the nonlinear evolution of tearing modes acting on initially small error-induced islands. Scaling predictions [3] for these effects indicate that the critical relative field error that can be tolerated becomes smaller as the tokamak becomes larger. In stellarators, the effect is more benign, as field errors appear only to cause increased plasma transport in the vicinity of islands. Great care has been taken to minimize magnetic field errors in the most recent generation of stellarator-type magnetic plasma traps [4–7]. These efforts stem from the realization that relative field errors of the order of $\Delta B/B \sim 10^{-2}$ (where the field error ΔB is applied in a toroidal field B) can form flux surface islands, leading to a more rapid loss of plasma.

In the past six years, several new and sensitive techniques have been developed to detect and map field errors [4, 7, 8–11]. These methods all rely on the detection of electrons injected along magnetic field lines. During the commissioning of ATF, flux surfaces were mapped using the fluorescent screen technique [4, 9]. Field errors were discovered and traced to uncompensated dipoles in the helical current feeds [4, 12]. Prior to elimination of these errors, plasma discharges indicated centrally peaked plasma profiles [13]. After correction of the uncompensated dipoles, flux surfaces were mapped a second time, and the island widths were found to be greatly reduced.

Field errors were then deliberately introduced using a set of perturbation coils that had been added to ATF, and electron-beam mapping of the flux surfaces showed that islands several centimeters in width could easily be created by these coils. After elimination of the error fields, the measured plasma temperature and density profiles were much broader. The field perturbation coils were then used to produce magnetic field asymmetries, and the measured plasma profiles were again shown to narrow as a result of islands.

Experimental results

Magnetic dipole coils separated by 180° were positioned on top of ATF's shell structure. Each dipole was located 1.1 m above the magnetic axis and consisted of 40 turns. The maximum current available for the dipoles was 6 kA, $I_{error}/I_{helical} = 20\%$ at $B_{z0} = 1$ T, or

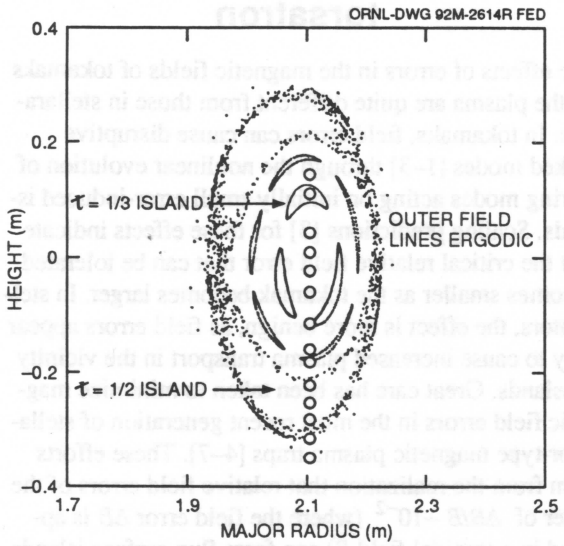

Fig. 1. Calculated flux surface islands formed when a perturbation of 0.7% on axis is applied (6 kA in the perturbation coil for a 1-T helical field). The locations of Thomson scattering data points are shown as circles.

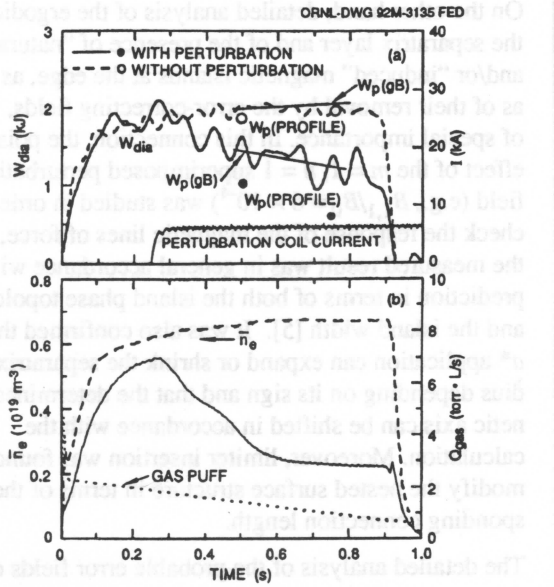

Fig. 2. (a) Diamagnetic stored energy as a function of time both with (solid line) and without (dashed line) a field perturbation after t = 0.25 s. Also shown are predictions of gyro-Bohm (W_p(gB)) scaling and the stored energy from Thomson scattering profile measurements. (b) The line-averaged density with and without the perturbation fields, and the gas puff flow rate. These measurements were made without feedback control of the gas puff.

$\tilde{B}_{Z0}/B_{\varphi 0} \leq 0.7\%$. Plots of the expected islands are shown in Fig. 1 at the toroidal angle of the Thomson scattering diagnostic. This plot shows that field lines beyond the $\iota = 1/2$ surface do not form closed flux surfaces. Plasma experiments were run with helical fields of 0.95 T on axis. The plasma was heated by 400 kW of 53-GHz microwave power.

A. Results without density control

Perturbing magnetic fields were introduced after stationary plasma conditions were established. Two types of experiments were performed: (1) the gas fueling was held constant; and (2) the line-averaged electron density was held constant by feedback control of the gas injection system. Measurements made without density control are discussed in this section. The results of turning on the error field at 0.25 s after the beginning of the shot are shown in Fig. 2. The stored energy (as measured by a diamagnetic loop) and the density decrease by a factor of two or more by the end of the discharge when compared to a discharge without applied perturbations. The density decay shown in Fig. 2(b) can be approximately characterized by two consecutive decay times of ~0.14 s: the first for the diffusion of the perturbing fields into the metal support structure, vacuum vessel and helical field coils, and the second for the subsequent field diffusion into the plasma. Figure 3 compares the electron temperature, density, and pressure profiles for shots with and without magnetic field perturbations at 0.5 s (0.25 s after the fields were perturbed). Following the perturbation the density dropped, resulting in a central temperature rise due to the microwave power being applied to fewer electrons. Note that the pressure profile became more peaked after initiation of the perturbation. Fits to the data were constructed by a data-fitting routine that symmetrized the temperature and density profiles about the plasma axis. The geometry used in this symmetrization is based on the vacuum magnetic surfaces without magnetic field perturbations. The plasma stored energy obtained from the Thomson scattering data of Fig. 3 is plotted at two points in Fig. 2(a) for both the perturbed and unperturbed cases and shows rough agreement with the diamagnetic signal. ATF experimental results [14, 15] have shown a strong dependence of the confinement time on the density, as characterized by gyro-Bohm or Large Helical Device (LHD) scaling, i.e., $\tau_E \sim n^{0.7}$. As shown in Fig. 3(a), the gross stored energy is within 15% of the values predicted by gyro-Bohm scaling.

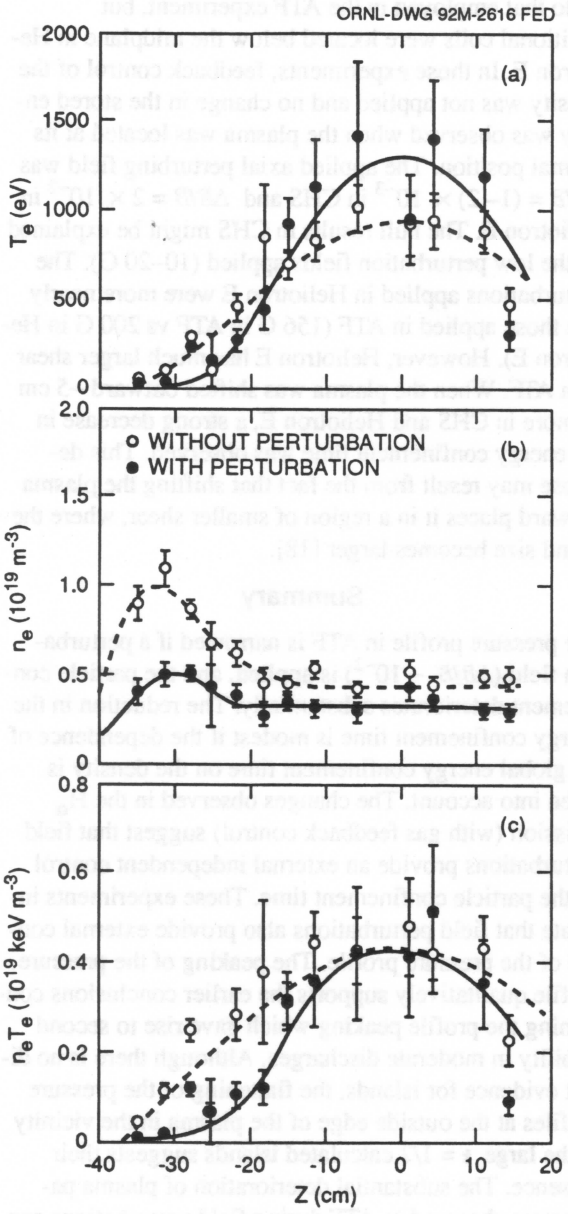

Fig. 3. Thomson scattering profile measurements of the temperature, density, and pressure both with and without a perturbation. The measurements were taken at 0.5 s (0.25 s after the perturbation was initiated). There was no gas feedback control.

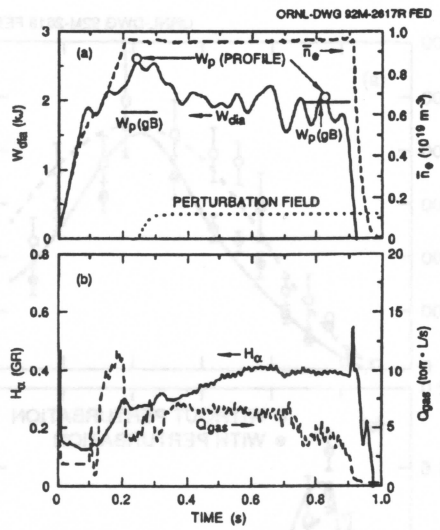

Fig. 4. (a) Diamagnetic stored energy as a function of time both with (solid line) and without (dashed line) a perturbation after t = 0.25 s. Also shown are predictions of gyro-Bohm (W_p(gB)) scaling and the stored energy from Thomson scattering profile measurements. (b) The H_α light emission measured at the wall and the gas puff flow rate. These measurements were made with feedback control of the gas puff, so that after an initial transient the density remained constant.

B. Results with density control

Figure 4(a) shows the stored energy and the density under conditions of density feedback control. The stored energy decreased by < 20% under these conditions, and the particle confinement time decreased by ~25% [i.e., an increase of ~25% in the H_α signal, Fig. 4(b)]. Slightly higher density discharges have shown a doubling of the H_α signal with no decrease in the stored energy. The central ECE electron temperature decreased slightly, and the ion temperature was almost constant after plasma initiation. The electron temperature, density, and pressure profiles are shown in Fig. 5. The electron temperature profile was narrowed and the density profile was altered only in the outer region of the plasma. The pressure profile became narrower with the perturbation, as shown in Fig. 5(c). The stored energy calculated from profile measurements is compared with the diamagnetic measurement just before the perturbation and near the end of the discharge in Fig. 4(a) and shows reasonable agreement. The stored energy predicted by gyro-Bohm scaling is also shown.

Comparison with other experiments

Profile data (Figs. 3 and 5) show that the plasma pressure remained constant near the axis after application of the field perturbation. However, in the (outer) region of the large $t = 1/2$ island, the pressure profile was reduced. This is consistent with the prior observation that similar

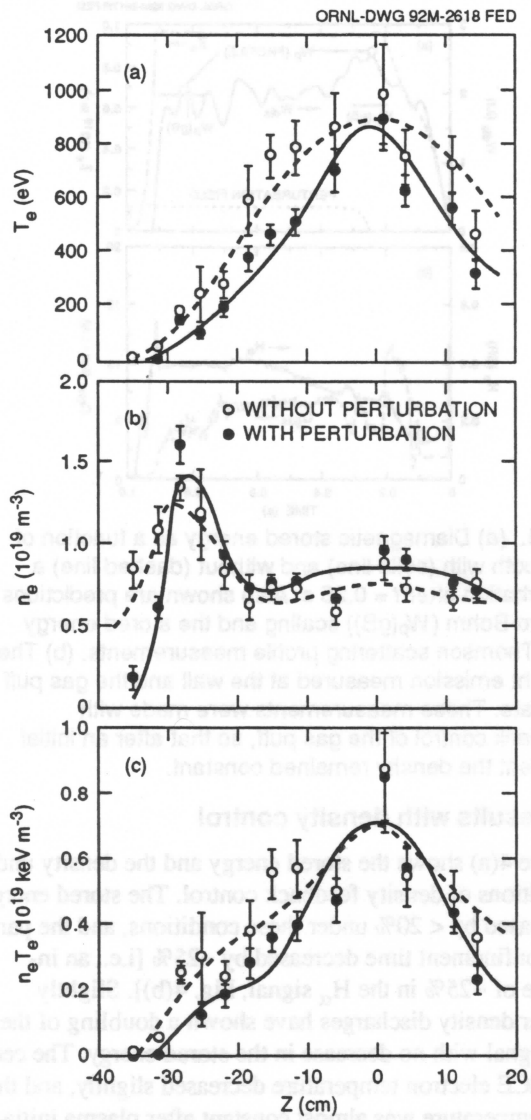

Fig. 5. Thomson scattering profile measurements of the temperature, density and pressure both with and without a perturbation. The measurements were taken at 0.75 s (0.5 s after the perturbation was initiated). Feedback control of the gas was applied to keep the density

perturbations in the original magnetic field coil system [4, 13] caused the plasma profiles to be peaked. The energy confinement time τ_E is observed to be directly dependent upon the density and changed only slightly when the density was held constant by feedback control of the gas puff. When feedback control was not applied, the density and the energy confinement time were almost halved. Although there was almost no effect on the potential at the limiter, the potential measured by the HIBP in the outer part of the plasma increased (with density feedback control). This would be expected if electrons preferentially escaped from the plasma region.

Similar experiments have been carried out on the Compact Helical System (CHS) and Heliotron E torsatrons [16–18] and in the TU-Heliac [19] but with quite different results. The geometry of the coils in CHS was similar to that employed in the ATF experiment, but additional coils were located below the midplane in Heliotron E. In those experiments, feedback control of the density was not applied and no change in the stored energy was observed when the plasma was located at its normal position. The applied axial perturbing field was $\Delta B/B = (1-2) \times 10^{-3}$ in CHS and $\Delta B/B = 2 \times 10^{-2}$ in Heliotron E. The null results in CHS might be explained by the low perturbation fields applied (10–20 G). The perturbations applied in Heliotron E were more nearly like those applied in ATF (156 G in ATF vs 200 G in Heliotron E). However, Heliotron E has much larger shear than ATF. When the plasma was shifted outward ~5 cm or more in CHS and Heliotron E, a strong decrease in the energy confinement time was observed. This decrease may result from the fact that shifting the plasma outward places it in a region of smaller shear, where the island size becomes larger [18].

Summary

The pressure profile in ATF is narrowed if a perturbation field ($\Delta B/B \sim 10^{-2}$) is applied, and the particle confinement deteriorates substantially. The reduction in the energy confinement time is modest if the dependence of the global energy confinement time on the density is taken into account. The changes observed in the H_α emission (with gas feedback control) suggest that field perturbations provide an external independent control on the particle confinement time. These experiments indicate that field perturbations also provide external control of the pressure profile. The peaking of the pressure profile qualitatively supports the earlier conclusions concerning the profile peaking which gave rise to second stability in moderate discharges. Although there is no direct evidence for islands, the flattening of the pressure profiles at the outside edge of the plasma in the vicinity of the large $\iota = 1/2$ calculated islands suggests their presence. The substantial deterioration of plasma parameters observed in ATF during field perturbations contrasts with the much smaller effects observed in other stellarator experiments.

Dick Colchin, Steve Aceto, Al England, Ralph Isler,
Masanori Murakami, Dave Rasmussen, Taner Uckan,
John Wilgen, and John Zielinski
Fusion Energy Division, Oak Ridge National Laboratory
P.O. Box 2009
Oak Ridge, TN 37831-8072, USA

Phone (615) 574-0982
FAX (615) 576-7926

[1] J. T. Scoville, R. L. LaHaye, et al., Nucl. Fusion **31** (1991) 875.
[2] A. W. Morris, R. Fitzpatrick, T. C. Hender., et al., in Controlled Fusion and Plasma Physics (Proc. 18th Eur. Conf. Berlin, 1991), **15C**, Part II, European Physical Society (1991) 61.
[3] R. Fitzpatrick, T. C. Hender, Phys. Fluids B **3** (1991) 644.
[4] R. J. Colchin, F. S. B. Anderson, A. C. England, et al., Rev. Sci. Instrum. **60** (1989) 2680 and references cited therein.
[5] H. Yamada, K. Matsuoka, S. Okamura, K. Ida, K. Nishimura, Rev. Sci. Instrum. **61** (1990) 686.
[6] G. G. Lysnyakov, E. D. Volkov, A. V. Georgievskij, et al., Study of the magnetic field configuration of an torsatron by the triode method and the luminescent rod method, submitted to Nucl. Fusion.
[7] R. Jaenicke, E. Ascasibar, P. Grigull, et al., Detailed investigation of the vacuum magnetic surfaces on the W7-AS stellarator, submitted to Nucl. Fusion.
[8] G. L. Hartwell, R. F. Gandy, M. A. Henderson, et al., Rev. Sci. Instrum. **59** (1988) 460.
[9] R. Takahashi, H. Matuura, T. Mizuuchi, et al., in Proc. 6th Int. Stellarator/Heliotron Workshop (Kyoto, 1986) Vol. 1, PPLK-006, Kyoto University, Kyoto, Japan (1986) 220.
[10] H. Haile, J. Massi, F. Schule, K. Schworer, H. Zwicker, in Controlled Fusion and Plasma Physics (Proc. 14th Europ. Conf. Madrid, 1987), **11D**, Part 1, European Physical Society (1987) 423.
[11] T. Y. Tou, B. D. Blackwell, L. E. Sharp, Rev. Sci. Instrum. **62** (1991) 1149.
[12] J. H. Harris, T. C. Jernigan, F. S. B. Anderson, et al., Fusion Technol. **17** (1990) 51.
[13] J. H. Harris, E. Anabitarte, G. L. Bell, et al., Phys. Fluids B **2** (1990) 1353.
[14] R. J. Colchin, M. Murakami, E. Anabitarte, et al., Phys. Fluids B **2** (1990) 1347.
[15] M. Murakami, S. C. Aceto, E. Anabitarte, et al., Phys. Fluids B **3** (1991) 2261.
[16] S. Okamura, L. Peranich, K. Matsuoka, et al., in Stellarators (Proc. 8th IAEA Tech. Committee Mtg. Kharkov, USSR, 1991), IAEA, Vienna (1991) Paper IV-P-5.
[17] S. Sudo, H. Zushi, K. Kondo, et al., Nucl. Fusion **31** (1991) 2349.
[18] O. S. Pavlichenko, Nucl. Fusion **32** (1992) 157.
[19] H. Watanabe, S. Kitajima, M. Takayama, T. Zama, in Stellarators (Proc. 8th Tech. Committee Mtg. Kharkov, 1991), IAEA, Vienna (1991) Paper IV-P-6.

People

Visitor to NIFS

Dr.V. D. Pustovitov from Kurchatov Institute, Moscow, Russia, visited National Institute for Fusion Science, Nagoya, Japan, from May 15 to September 11 under the guest researcher program of the Ministry of Education. He made significant contributions to the CHS program, especially in the analysis of diamagnetic flux in the low-aspect-ratio helical plasma.

Keisuke Matsuoka
Institute for Fusion Science
Nagoya, 464-01, Japan

Reactor Studies

Divertor field line mapping in Helias configurations

Investigations of various vacuum magnetic fields of Helias configurations allowed a divertor concept to be developed [1,2] for Helias-type stellarators such as the planned Wendelstein 7-X stellarator (major radius: R_0 = 5.5 m, number of periods N = 5): five helical troughs are located at a distance of one-fifth of the plasma radius outside the plasma tube along the so-called helical edges, as shown in Fig. 1.

Tracing a large number of magnetic field lines from the outer neighborhood of the LCMS (last closed magnetic surface) showed that these helical troughs provide complete separation of the magnetic field lines starting at the plasma and ending at the divertor troughs from the field lines starting at the first wall. This separation is independent of the detailed fixed-point behavior and is preserved when diffusion is taken into account.

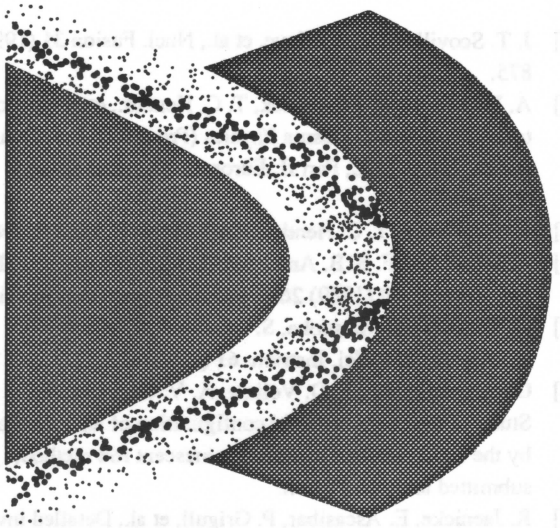

Fig. 2. Part of the triangular cross section. The right gray area marks the position of the helical trough, the small and large points characterize three consecutive layers formed by the field lines, and the left gray area indicates the outboard part of the plasma.

For this divertor concept to be viable in an experimental device, the following properties of Helias configurations are advantageous. Configurational flexibility with respect to rotational transform ($5/6 \lesssim \iota_{edge} \lesssim 5/4$) can be achieved together with near-invariance in space of

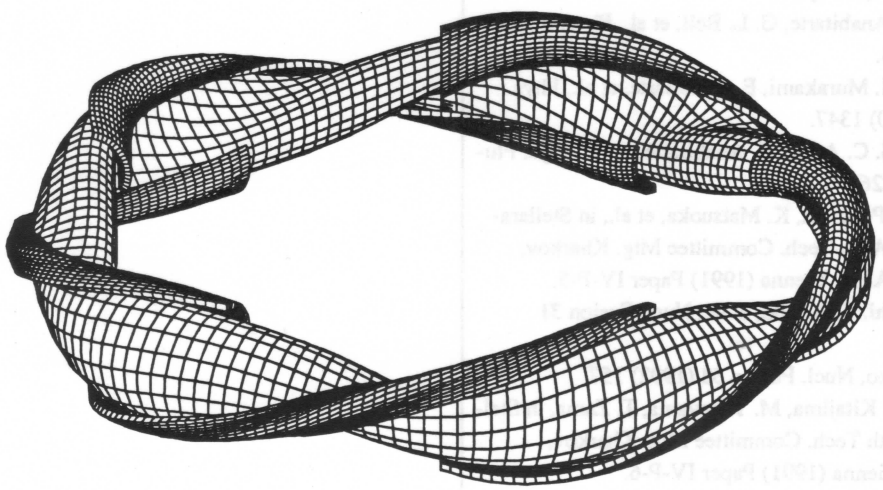

Fig. 1. Plasma surface with helical troughs, each somewhat longer than a single period.

the helical edges. The same near-invariance holds with respect to the independence of the equilibrium beta value.

With the divertor plates defined, the field line structure in the outer neighborhood of the LCMS is investigated from a complementary point of view: the map of the troughs onto themselves which is given by the field lines starting on the troughs is investigated [3]. When these field lines are ordered according to their minimum distance from the plasma boundary, ordered layers are found, as shown in Fig. 2. The magnetic field lines forming the different layers map ordered areas on the helical troughs onto each other (see Fig. 3).

The field lines forming the innermost layer intersect the plasma-facing surfaces of the helical troughs in a pattern which is concentrated along the position of the helical edge. This part of the intersection pattern is surrounded by areas formed by field lines of the outer layers. Figures 2 and 3 are complementary representations. Together they illustrate the nature of the map between the troughs: ordered areas on the troughs correspond to ordered layers in the edge region.

Jürgen Nührenberg, Erika Strumberger
Max Planck Institut für Plasmaphysik
D8046, Garching bei Muenchen, FRG
Phone (49)-89-3299-1368
FAX: (49)-89-3299-2579

[1] E. Strumberger, Nucl. Fusion **32** (1992) 737.
[2] J. Nührenberg, E. Strumberger, Contr. to Plasma Physics **32** (3-4) (1992) in press.

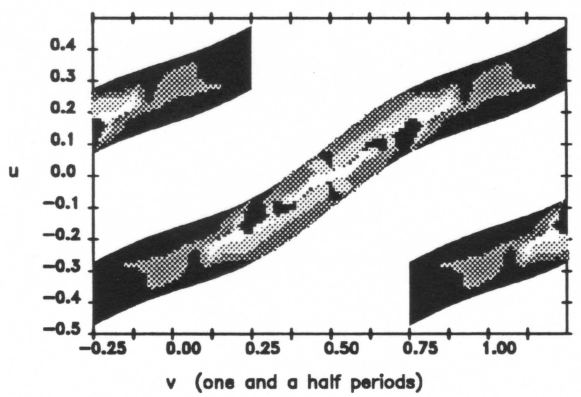

Fig. 3. Intersection pattern of the magnetic field lines ordered according to their minimum distance from the plasma boundary. The white areas belong to the field lines forming the innermost layer, while the darkest ones belong to the outermost layer. The framed areas mark the positions of the helical troughs.

Proposals

HSX proposal

The Torsatron/Stellarator Laboratory at the University of Wisconsin–Madison has submitted a proposal to the U.S. Department of Energy for the construction and operation of a new modest-sized stellarator experiment. The proposed device, HSX (Helically Symmetric Toroidal Experiment), is based on the concept of quasi-helically symmetric equilibria developed by Nührenberg and Zille at the Max-Planck Institut für Plasmaphysik in Garching, Germany.

Quasi-helically symmetric stellarators, to a good approximation, possess a direction of symmetry in magnetic coordinates and are therefore nearly topologically equivalent to a tokamak without plasma current. In effect, the field structure is a 'hybrid' of the axisymmetric and stellarator concepts, combining the good particle containment of the axisymmetric system with the advantage of no required plasma current in the stellarator.

HSX is a four-field-period device with an aspect ratio of 8; it is based on a modification of the QH48 design developed by Nührenberg at Garching. The magnetic well has been increased to a peak value of –0.6% (at 80% radius) with virtually no increase in the nonhelical spectral components of B. The toroidal curvature term in the spectrum of B corresponds to the toroidal curvature in an unoptimized device at an aspect ratio greater than 240. As such, there are no superbanana direct-loss orbits, and neoclassical transport is directly analogous to, and reduced, from that in an equivalent axisymmetric tokamak. Monte Carlo diffusion coefficients are nearly

HSX Device Parameters

Major radius	1.2 m
Minor radius	0.15 m
Average plasma volume	~ 0.44 m^3
Number of periods	4
Rotational transform	~1.05 axis; <1.12 edge
Peak magnetic well depth	–0.6%
Number of coils/period	12
Average coil radius	~ 0.3 m
Axis magnetic field strength	1 T
Magnet pulse length	0.6 s

two orders of magnitude below a conventional helical system and, because of the reduced banana widths, a reduction in anomalous transport (by a factor of three as compared to an equivalent tokamak) is implied by Lackner scaling.

The device parameters are summarized in the accompanying table.

HSX plasmas will take advantage of 28-GHz gyrotrons to obtain hot-electron plasmas capable of operation in a low collisionality regime. It is easier to obtain a collisionless plasma in a quasi-helically symmetric stellarator than in a conventional stellarator or tokamak because of the shorter connection length for the bounce motion. Expected plasma parameters with 200-kW (source), 28-GHz ECH are:

Power density	0.45 W/cm^3
Electron density (peak)	1×10^{13} cm^{-3}
Central electron temperature (LHD scaling, 100 kW absorbed power)	700 eV
Energy confinement time (LHD scaling)	2 ms
Peak beta	0.3%
Electron collisionality	< 0.1

At the operational parameters of HSX, finite beta effects result in only small changes to the magnetic field spectrum and the bootstrap current is predicted to be less than 600 A, resulting in the introduction of no dangerous resonances in the rotational transform. Flexibility in the magnetic parameters and the ability to change the magnetic field spectral content to increase neoclassical transport for physics studies are obtained through use of a set of small trim coils.

Because HSX bridges the gap between asymmetric currentless stellarators and symmetric current-driven tokamaks, it will provide a unique opportunity to explore some key fundamental physics questions that underlie these two leading contenders in the fusion program. Principal among these questions are the role of the electric field in plasma transport; the controversy regarding plasma spin-up, rotation, and momentum damping in symmetric vs nonsymmetric configurations (with possible insight into L-H transitions); density and temperature profiles under tokamak-like and stellarator-like modes of operation; and the effects of reduced banana widths and magnetic well structure on anomalous transport.

David T. Anderson
Torsatron-Stellarator Laboratory
University of Wisconsin
Madison, Wisconsin 53706

Phone (608) 262-0172
FAX (608) 262-1267